Article

Not peer-reviewed version

Biological Synthesis and Characterization of Silver-Doped Nanocomposites: Antibacterial and Mechanistic Studies

Franklin Loic Tchinda Taghu , Boniface Pone Kamdem , Vincent Ngouana , Zuriatou Yajep Tanka , Victorine Lorette Yimgang , Julius Nsami Ndi * , Paul Keilah Lunga * , Fabrice Fekam Boyom

Posted Date: 25 October 2023

doi: 10.20944/preprints202310.1616.v1

Keywords: silver nanomaterials; activated carbon; infectious diseases; antibacterial mechanism of action; cytotoxicity

Article

Biological Synthesis and Characterization of Silver-Doped Nanocomposites: Antibacterial and Mechanistic Studies

Franklin Loic Tchinda Taghu [1], Boniface Pone Kamdem [1,2], Vincent Ngouana [3], Zuriatou Yajep Tanka [1], Victorine Lorette Yimgang [1], Julius Nsami Ndi [4,*], Paul Keilah Lunga [1,*] and Fabrice Fekam Boyom [1]

[1] Antimicrobial and Biocontrol Agents Unit (AmBcAU), Laboratory for Phytobiochemistry and Medicinal Plants Studies, Department of Biochemistry, Faculty of Science, University of Yaoundé I, Yaounde P.O. Box 812, Cameroon; Email: loicfrank120@gmail.com (FLTT), ponekamdemboniface@gmail.com (BPK), zuriayajeh@gmail.com (ZYT), vyimgang@yahoo.fr (VLY)

[2] Higher Institute of Agriculture, Forestry, Water and Environment (HIAFWE), University of Ebolowa, P.O. Box 755, Ebolowa-Cameroon; Email: ponekamdemboniface@gmail.com (BPK),

[3] Department of Pharmacy, Faculty of Medicine and Pharmaceutical Sciences, University of Dschang, Cameroon; Email: ngouanavincent@yahoo.fr (VN),

[4] Applied Physical and Analytical Chemistry Laboratory, Department of Inorganic Chemistry, Faculty of Science, P.O. Box 812 Yaounde, University of Yaounde I, Cameroon; Email: ndinsami2002@gmail.com (JNN)

* Correspondence: lungapaul@yahoo.ca (PKL); Tel.: (+237) 672 46 01 30; ndinsami2002@gmail.com (JNN); Tel.: (+237) 677807132.

Abstract: In this study, we report the antibacterial mechanisms of action of uniform silver nanoparticles (AgNPs) and decorated activated carbon nanocomposite (CAC-AgNPs) obtained using a green synthesis approach. The nanomaterials were characterized by ultraviolet-visible (UV-vis) absorption spectra and Fourier transform infrared (FTIR) spectra. The antibacterial activity of the as-prepared nanomaterials was evaluated against an array of bacterial strains by microdilution method, whereas their cytotoxicity profile was evaluated on Vero cells (human mammalian cells). The antibacterial mechanistic studies of active nanomaterials were carried out through bacterial growth kinetics, nucleic acid leakage test, and catalase inhibition assay. A silver nanocomposite was successfully fabricated from *Croton macrostachyus*-based activated carbon. The as-prepared nanomaterials exhibited antibacterial activity against an array of bacterial strains (minimum inhibitory concentration (MIC) range: 62.5 to 500 µg/mL), the most susceptible being *Escherichia coli* and *Staphylococcus aureus*. Cytotoxicity studies of the nanomaterials on Vero cells revealed that the nanocomposite (median cytotoxic concentration (CC_{50}): 213.6 µg/mL) was less toxic than the nanoparticles (CC_{50} value: 164.75 µg/mL) counterpart. Antibacterial mechanistic studies unveiled that the nanomaterials induced (i) bacteriostatic activity vis-à-vis *E. coli* and *S. aureus* and (ii) inhibition of catalase in these bacteria. This novel contribution on the antibacterial mechanisms of action of silver nanocomposite from *C. macrostachyus*-based activated carbon might contribute to the understanding of antibacterial action of these biomaterials. Nevertheless, more chemistry and *in vivo* experiments, as well as in depth antibacterial mechanistic studies are warranted for the successful utilization of these antibacterial biomaterials.

Keywords: silver nanomaterials; activated carbon; infectious diseases; antibacterial mechanism of action; cytotoxicity

 doi:10.20944/preprints202310.1616.v1

1. Introduction

Diseases that spread from one person to another and are caused by bacteria, parasites, fungi, and viruses are termed as infectious diseases [1]. Noteworthy, infectious diseases are also transmitted through bug bites, contaminated food, water and soil, as well as poor sanitation [2]. Common infectious diseases include common cold, flu (influenza), stomach flu (gastroenteritis), hepatitis, respiratory syncytial virus (RSV) and COVID 19 [2]. Infectious diseases have a parade number of symptoms or manifestations that may lead to death, if the concerned illnesses are left untreated. Infectious diseases are one of the significant causes of morbidity and mortality across the world. Generally, antibiotics are used to diagnose, treat or prevent bacterial infections; however, mutations resulting from their use might cause bacterial drug resistance [3]. Remarkably, bacteria has seemingly won the battle against antibiotics since most of them have become resistant to these drugs [4]. It is important to mention that various antimicrobial agents interferes with (i) synthesis of cell wall, (ii) ribosomal function, (iii) folate synthesis, (iv) biofilm formation and (v) nucleic acid synthesis [5–9]. Resistance occurs when there are profound modifications to one of these functions. For instance, bacterial resistance to β-lactam antibiotics include modification of porins (cell wall proteins) and targets, production of the inactivating enzymes namely beta-lactamases and autolytic enzymes' inactivation [10]. Inhibition of nucleic acid synthesis is observed with quinolones and fluoroquinolones that target DNA synthesis through inhibition of type 2 topoisomerases, such as DNA gyrase and topoisomerase IV [11]. Sulfonamides, such as trimethoprim, which is widely used to treat urinary tract infections and pneumonia binds on dihydrofolate reductase to inhibit the synthesis of folic acid [12]. In addition, the ribosomal function is affected by macrolide antibiotics [13]. Aminoglycosides and quinolones have been shown to inhibit biofilm formation by *Pseudomonas aeruginosa* [14,15]. These bacterial drug resistance events, combined with the problem of toxicity, high cost and unavailability of modern therapy justify the crucial need to search for new and safe antimicrobials. Infectious diseases cause over 4.8 % of mortality rate and an economic loss of more than USD 100 trillion per year worldwide worldwide [16]. Since their introduction into health care and clinical practice in the early 20th century, with the discovery of penicillin in 1928, antibiotics have revolutionized medicine, many of them have been either isolated from natural products or chemically synthesized and numerous lives have been saved [17]. It is noted that, these drugs are increasingly threatened by bacteria that develop a wide variety of resistance mechanisms. Medicinal plants remain the most abundant natural source of active drugs and are invaluable in the traditional treatment of a number of infectious diseases since time antediluvian [18,19]. In fact, medicinal plants have been reported to contain numerous secondary metabolites, including terpenoids, flavonoids, phenolic compounds, alkaloids, tannins, saponins, among others. These metabolites have been reported to inhibit the growth of several microorganisms, including bacteria (*Staphylococcus aureus*, *Escherichia coli*, *Pseudomonas aeruginosa*, *Shigella* spp., etc.).

However, the incorporation of these plant secondary metabolites into nanosized particles has been proven more valuable as this nanosize form can overcome biological barriers and augment the delivery of active principles to the target site thereby increasing the efficacy [20,21]. Undoubtedly, one of the latest approaches to combat resistant microorganisms include the use of nanotechnology-based antimicrobials [22,23]. Because of the non-specific mechanistic action of metal-based nanoparticles on bacteria, the development of resistance by these microorganisms is difficult. Thus, resistance to antibiotics is not relevant to nanoparticles (NPs) as there is a direct contact with the bacterial cell wall without the need of penetration into microbial cells [23]. Nanoparticles are spherical particles (size: 1-100 nm) that exhibit unique properties due to their high surface area to volume ratio. They can be classified into fullerenes and metal, ceramic, and polymeric NPs [24]. In addition, nanoparticles are bioactive products that are stable, dispersed, biocompatible and affordable [25]. Dakal et al. [26] revealed that silver nanoparticles are able to adhere onto the surface of cell wall or membrane, penetrate inside the cell and damage organelles, such as ribosomes, mitochondria and vacuoles by releasing free ions to produce reactive oxygen species (ROS) [26,27]. The metal used for the fabrication of nanoparticles undergo a reaction with chemical groups of components of the cell membrane (phosphorus and sulfur groups), such as proteins, lipids, and DNA

Preprints (www.preprints.org) | NOT PEER-REVIEWED | Posted: 25 October 2023 doi:10.20944/preprints202310.1616.v1

bases to generate potential reactive oxygen species [28]. It has been reported that the accumulation of nanoparticles within bacterial cell walls and membranes can induce morphological changes in the bacteria. These include membrane detachment and disruption, shrinkage of cytoplasm, and formation of electron-dense holes [17]. The preparation of nanocomposites using activated carbons contributes to increasing the antibacterial action of these products. Because of their light weight, high specific surface areas and favorable electrical and mechanical properties, nanocarbons have recently gained considerable attention [29]. In fact, activated carbon is a porous material with amphoteric characteristics, which is used for the adsorption of organic and inorganic compounds [30]. The high content in oxygen onto the surface of activated carbons is crucial for an effective adsorption of bacteria, such as *S. aureus* and *E. coli* [31]. Parameters, such as pore size distribution, surface area, pH, and elemental analysis are used to characterize active carbon products [31,32]. Recent studies have demonstrated that activated supported metal nanoparticles prepared from plant (*Cassia roxburghii*, *Aloe vera* and *Cinnamomum verum*) extracts afford nanocomposites with superior antibacterial efficiency [33–35].

Based on the foregoing considerations, the present study aims to use *Croton macrostachyus* (a plant employed in the traditional treatment of a number of infectious diseases, including malaria and venereal diseases, among others) for the fabrication of carbon activated immobilized metal nanoparticles. Moreover, antibacterial screening of the fabricated nanocomposite and potential mechanistic basis of antimicrobial action are investigated.

2. Results and Discussion

2.1. Physical and UV-Vis Analysis of the Nanoparticles

A green synthesis of silver nanoparticles was successfully achieved using aqueous extract of *C. macrostachyus* stem bark along with a solution of silver nitrate ($AgNO_3$). The change in color observed from pale yellow to dark brown indicated the formation of the nanoparticles (Figure 1). The fabrication of the AgNPs was further confirmed by UV-vis visible spectroscopy in a wavelength range of 350-900 nm as described in Figure 2. On the spectrum of AgNPs, a spectrophotometric absorption peak was observed at a characteristic wavelength of 443 nm and was attributed to the surface plasmon resonance of the formed nanoparticles. Meanwhile, the spectra of the silver salt and aqueous extract solutions of *C. macrostachyus* showed no peaks. For silver nanoparticles, the λmax values were obtained in the wavelength range of the visible spectrum (400-500 nm) [36]. These results are consistent with a number of studies published on the synthesis of nanomaterials from other plants with wavelength values corresponding to the visible spectrum as for the aqueous extract of *C. sparsiflorus* (457 nm ; Kathiravan et al. [37]) and *C. bonplandianum* (415 nm ; Kapoor [38]).

(a) (b)

Figure 1. Pictorial representation of the prepared extract (a) and silver nanoparticles (b) from *C. macrostachyus* stem bark.

Preprints (www.preprints.org) | NOT PEER-REVIEWED | Posted: 25 October 2023 doi:10.20944/preprints202310.1616.v1

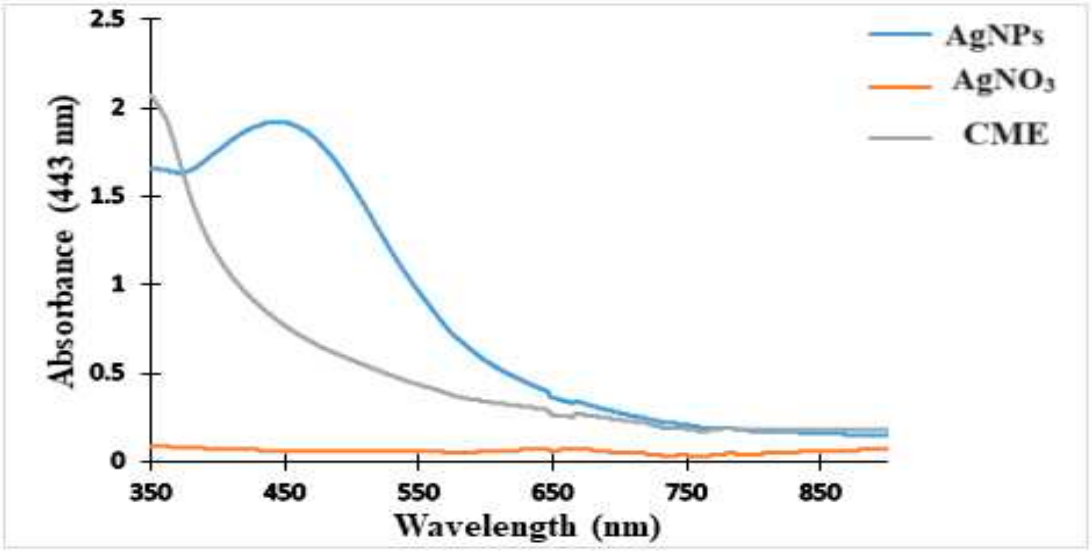

$AgNO_3$, chemical reagent (silver nitrate); **AgNPs**, silver nanoparticles; **CME**, *Croton macrostachyus* extract.

Figure 2. UV–Vis spectra of *C. macrostachyus* extract (CME) and nanoparticles (**AgNPs**) *vs.* chemical reagent ($AgNO_3$).

2.2. FTIR Analysis C. Macrostachyus Extract and the Nanoparticles

To identify the plausible functional groups that are involved in the reduction of silver ion to AgNPs, FTIR spectroscopy was performed on the as-prepared extract (*C. macrostachyus* extract) and nanoparticles (AgNPs). The FTIR spectrum (Figure 3) of the aqueous extract of *C. macrostachyus* (blue color), shows a peak at 511 cm^{-1}, which corresponds to the band of alkyl halides. The distortion observed at 781 cm^{-1} may be related to the CH=CH bonds of the benzylic aromatic ring of phenols, whereas the presence of an intense peak at 1021 cm^{-1} is characteristic of an aliphatic amine (C-N). At 1304 cm^{-1}, a weak peak, which is characteristic of C-OH groups is observed, whilst another intense peak that corresponds to the C=O groups of protein amides is detected. Moreover, two distinct peaks, which were identified at 2912 cm^{-1} and 3287 cm^{-1} are potentially linked to the symmetrical elongation vibrations of the CH_2–CH_3 group of an alkane and the O-H bonds linked to alcohols and phenolic compounds, respectively. These chemical groups are well known to exist in plant extracts as evidenced by previously published research papers [39–41]. The FTIR spectrum (orange color) of AgNPs revealed major peaks at wavelength 3300 cm^{-1} (OH bond stretching) and 1634 cm^{-1} (carbonyl C=O group), which corresponded to the involvement of hydroxyl and carboxylic acid moieties (encountered in polyphenols, phenolic acids and proteins) of *C. macrostachyus* extract in the reduction of the silver ions (Ag^+). Noteworthy, primary (proteins) and secondary (polyphenols) metabolites are responsible for the formation and stabilization of silver nanoparticles (AgNPs) [42,43].

As evidenced by the characteristic peak revealed at 1634 cm^{-1}, the presence of proteins prevented the agglomeration of the as-prepared nanoparticles. Indeed, it has been reported that capping proteins prevents agglomeration in the medium and are responsible for the fabrication of highly stable AgNPs [44]. As already reported by other authors [45,46], the absence of peak, which is characteristic to the Ag-O groups, indicates that silver is present in metallic form in the fabricated nanoparticles [45,46]. These results demonstrated that *C. macrostachyus* extract contains secondary metabolites, such as phenolics, flavonoids, alkaloids, and terpenoids, among others [47], which might have been incorporated into the prepared nanoparticles.

Preprints (www.preprints.org) | NOT PEER-REVIEWED | Posted: 25 October 2023 doi:10.20944/preprints202310.1616.v1

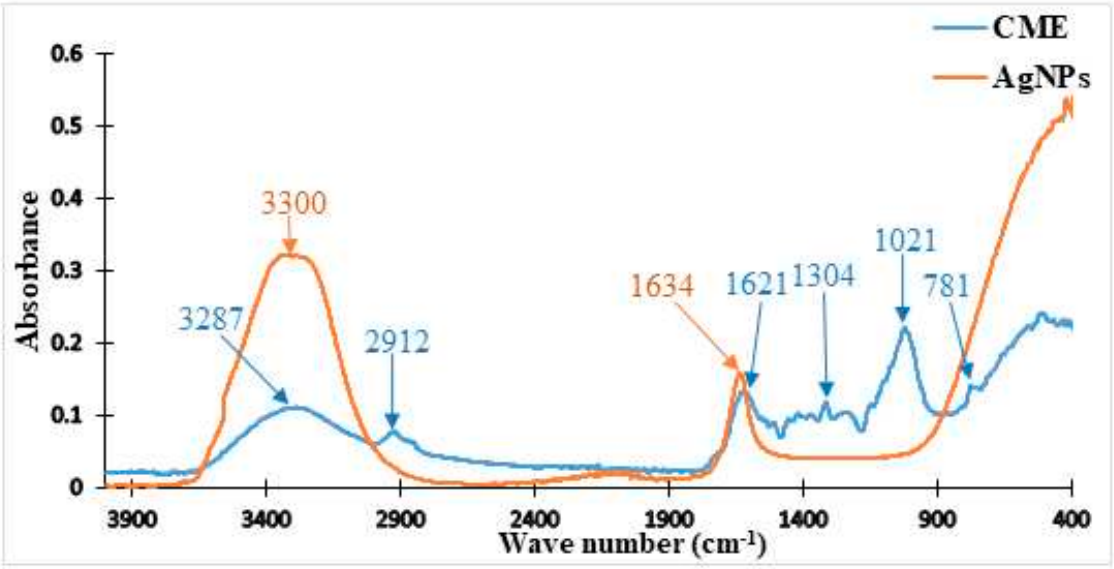

AgNPs, silver nanoparticles; **CME**, *Croton macrostachyus* extract.

Figure 3. FTIR spectra of extract (CME) and nanoparticles (AgNPs) prepared from *C. macrostachyus* stem bark.

2.3. Characterization of the As-Prepared Activated Carbon and Nanocomposite

2.3.1. FTIR of the Activated Carbon

Figure 4 shows the IR spectra of the activated carbon (orange color) and *C. macrostachyus* dried powder (blue color). It appears that both spectra are different in number and type of peaks. The very broad band observed around 3200-2500 cm^{-1} is attributed to the O-H elongation vibration association, and may be characteristic of carbonyl and phenolic hydroxyl groups. The peak observed at 1574 cm^{-1} is characteristic of C=C alkene groups of benzene. The frail peak that appeared at 1156 cm^{-1} might be attributed to the P-O elongation from the phosphoric acid used in the activation. Another weak signal peak, which appeared at 1071 cm^{-1} corresponds to the in-plane deformation of the C-O grouping of the aromatic compounds and acetyl and carboxylic acid functions. The peaks that appeared at 988 and 876 cm^{-1} indicate the presence of meta and di-substituted benzene groups. Moreover, the presence of a haloalkane was indicated by the signal observed at 488 cm^{-1}. Noteworthy, the peaks, which were observed with the plant dried powder at 3287 and 2921 cm^{-1} disappeared after carbonization. In addition, the peak position was shifted to lower regions when *C. macrostachyus* dried powder was treated with phosphoric acid (H_3PO_4). The observed structural modifications have been attributed to the presence of organophosphorus compounds, which might overlay the outside plane deformation vibrations of C-H in the aromatic moieties [48].

Preprints (www.preprints.org) | NOT PEER-REVIEWED | Posted: 25 October 2023 doi:10.20944/preprints202310.1616.v1

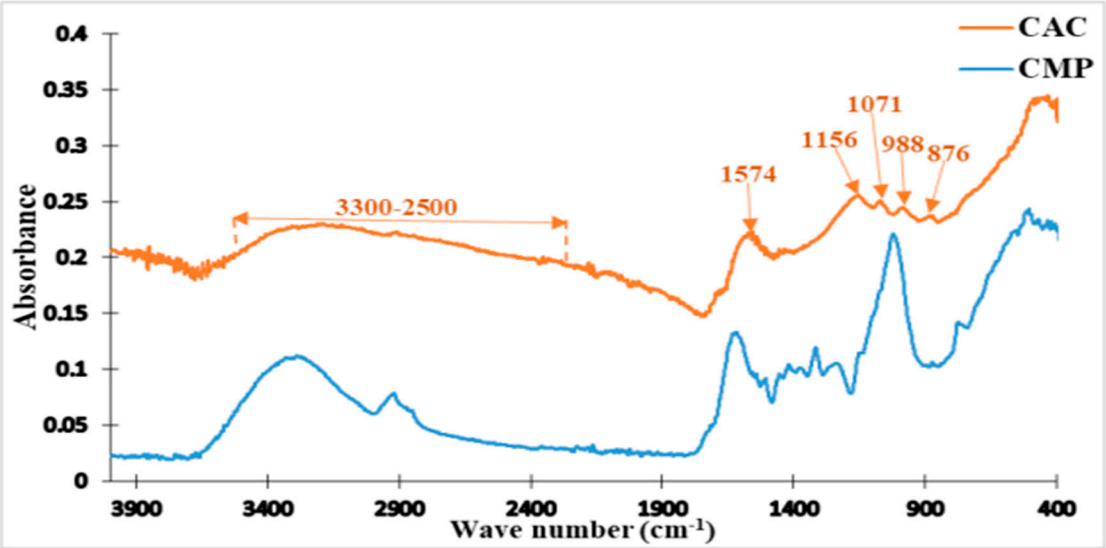

CAC, activated carbon; **CMP**, *Croton macrostachyus* dried powder.

Figure 4. FTIR spectra of *C. macrostachyus* dried powder (CMP) and activated carbon (CAC).

2.3.2. FTIR of the Doped-Activated Carbon (Nanocomposite)

Figure 5 reveals the spectrum of the fabricated nanocomposite (orange color) compared to that obtained from the activated carbon (blue color). It can be seen that both spectra are having almost the same pattern, thus indicating that the obtained nanocomposite is not a hybrid material and is structurally identical to the nanoparticle. A number of research groups have obtained the same results while working on the green synthesis of nanofillers and their nanocomposites [49,50].

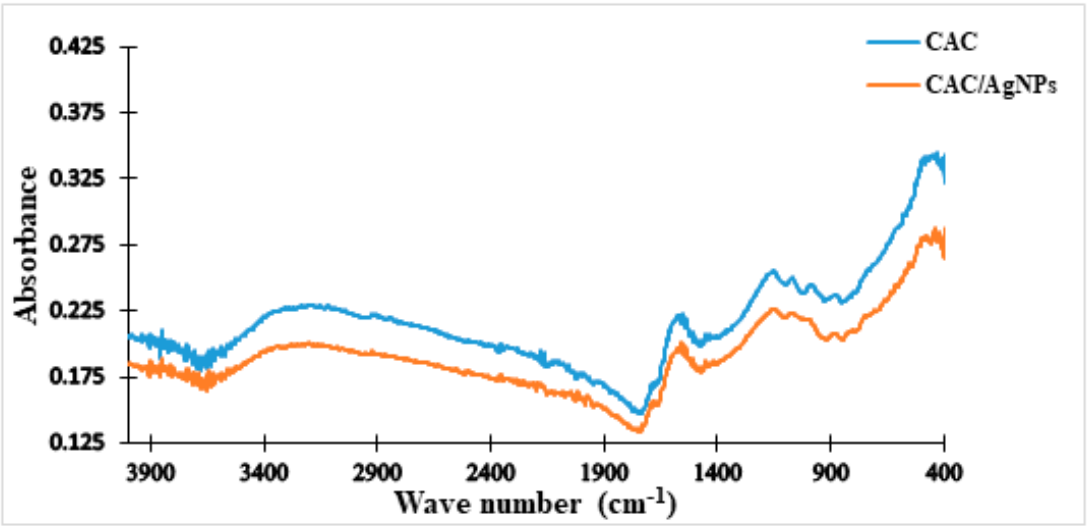

CAC, activated carbon; **CAC/AgNPs**, nanocomposite.

Figure 5. FTIR spectra of the activated carbon (CAC) and nanocomposite (CAC/AgNPs).

2.3.3. Iodine Number and Methylene Blue Index

The identification of the iodine number and methylene blue index tests allowed for the characterization of microporosity (iodine), mesoporosity and macroporosity (methylene blue) of the activated carbon and nanocomposite. Figure 6 shows the values of the iodine number and methylene blue index of activated carbon and nanocomposite. The results demonstrated that the iodine number

Preprints (www.preprints.org) | NOT PEER-REVIEWED | Posted: 25 October 2023 doi:10.20944/preprints202310.1616.v1

of the activated carbon (1026.69 mg/g) is higher than that of the nanocomposite (975.29 mg/g). These values corroborate with those obtained by Islam et al. [51] (iodine number : 1000-1200 mg/g) and Raut et al. [52] (iodine number : 1140.69 mg/g) in their work on the fabrication and characterization of activated carbon from Jute Stick, and sugarcane bagasse and rice husk, respectively [51,52]. Furthermore, the values of the methylene blue indices were almost identical for the activated carbon (89.862 mg/g) and nanocomposites (89.854 mg/g).

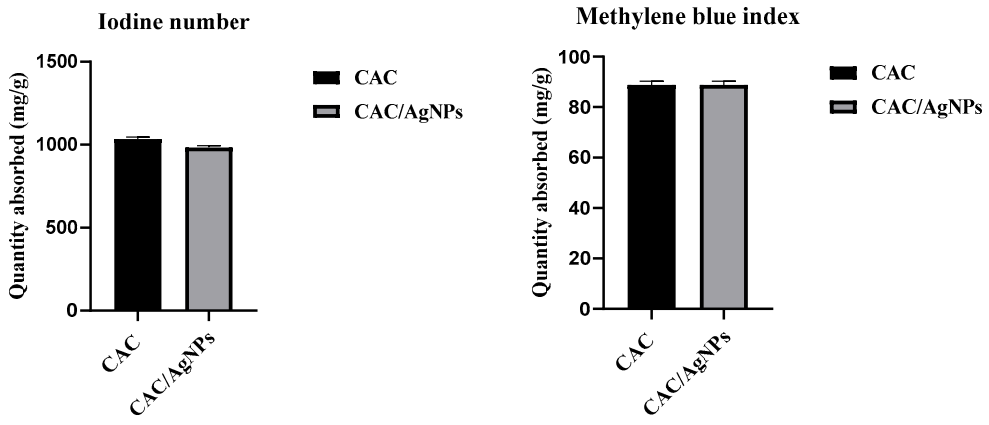

CAC : activated carbon ; CAC/AgNPs : silver-doped nanomaterial ; Data are represented as mean ± standard deviation. The histograms assigned to the stars are significantly different ($p < 0.0001$, Paired t-test).

Figure 6. Quantitative analysis of iodine number and methylene blue index of activated carbon and nanocomposite thereof.

As a partial conclusion, aqueous extract, silver nanoparticles, activated carbon and derived nanocomposites were successfully prepared from the stem bark of *Croton macrostachyus*. UV-visible spectra confirmed the synthesis of the nanoparticles. FTIR analysis revealed the presence of chemical functional groups that are characteristic to nanomaterials [53]. Noteworthy, the effect of the temperature and the activating agent (i.e. phosphoric acid) during the carbonization process (depolymerization and dehydratation) was clearly demonstrated by the difference in the spectra of the *Croton macrostachyus* extract and activated carbon [54]. In addition, there were no significant changes in the spectra obtained for CAC and CACAgNPs confirming the fabrication of the nanocomposite through van der waals interactions [55]. Furthermore, the percentage of iodine number was decreased by 5%, whereas the methylene blue index showed percent reduction of 0.008% inferring that, in lieu of macrospores, the activated carbon's microspores constituted the main fixation site for the nanoparticles, leading to a decrease in their adsorption surface [45,56].

2.4. Antibacterial and Cytotoxic Activity

2.4.1. Minimum Inhibitory Concentration

Table 1 summarizes the MIC values (range : 62.5 µg/mL to >1000 µg/mL) of *C. macrostachyus* extract, and the as-prepared activated carbon, nanoparticles and nanocomposites. The median cytotoxic concentrations (CC_{50}s) of these entities on Vero cells are also presented in Table 1. The silver nanoparticles were the most active (MIC range : 62.5 to 125 µg/mL), followed by the nanocomposites (MIC range : 125 to 500 µg/mL). Although the nanocomposites were less active than the derived nanoparticles, their activity was superior when compared to that of the activated carbon (MIC > 1000 µg/mL). In fact, the antibacterial activity of activated carbon (MIC > 1000 µg/mL) was potentiated by that of the incorporated nanoparticles. To our knowledge, no report has previously described the involvement of silver nanoparticles in potentiating the antibacterial activity of activated carbon obtained from the aqueous extract of *C. macrostachyus* stem bark. On the other hand, metal

Preprints (www.preprints.org) | NOT PEER-REVIEWED | Posted: 25 October 2023 doi:10.20944/preprints202310.1616.v1

nanoparticles are generally thought to be toxic because of the metal used during the fabrication as a result of their large specific surface area, high surface energy and magnetic interaction, as well as their easiness to agglomerate into micron- or millimeter-sized floccules [57]. Therefore, we attempted to overcome or minimize the toxicity caused by nanoparticles while maintaining the antibacterial activity by preparing the nanocomposites counterpart using an activated carbon.

Table 1. Minimum inhibitory (MIC) and median cytotoxic (CC_{50}) concentrations.

	MICs (µg/mL)					CC_{50s} (µg/mL)	Selectivity indices (SI)
	E. coli	*S. flexneri*	*S. sonnei*	*S. enteridis*	*S. aureus*		
CME	>1000	>1000	>1000	>1000	>1000	>1000	
CAC	>1000	>1000	>1000	>1000	>1000	396.5 ± 3.11	ND
AgNPs	62.5	125	125	125	125	164.75 ± 12.51	~2.64
CAC/*AgNP*	125	500	500	500	250	213.6 ± 1.41	~1.70
Ciprofloxacin	0.078	0.078	0.078	0.156	0.039	-	
Podophyllotoxin						0.4 ± 0.1	

AgNPs: Silver nanoparticles; **CAC**: Activated carbon; **CAC/AgNP**: Doped activated carbon; **CME**: Aqueous extract of *C. macrostachyus.* **ND:** Not determined.

2.5. Effect of the As-Prepared Nanomaterials on the Mortality Kinetics of S. aureus and E. coli

The growth of *E. coli* and *S. aureus* was monitored in the presence of nanoparticles (AgNPs) and nanocomposites (CAC/AgNPs) at a series of MIC value-based concentrations, including MIC/4, MIC/2, MIC, 2MIC and 4MIC for 24 h. As a result, both nanomaterials inhibited the growth of *E. coli* and *S. aureus* at MIC, 2MIC and 4MIC (Figures 7 and 8). Referring to figure 7 A & B, treatment with AgNPs decreased the bacterial population after 2 to 4 h of incubation time, followed by a stationary state of bacterial growth from 4 to 10 h of incubation time. In figure 8 A & B, the same trend was observed with the treatment using various concentrations of the nanocomposites (CAC/AgNPs). In fact, after 4 h incubation time, there was a bacterial growth, which was followed by a 6 h period (from 4 to 10 h incubation time) of no growth. From 10 h onwards, both *E. coli* and *S. aureus* resumed an exponential growth up to 24 h of incubation time upon treatment with both nanomaterials. The ephemeral bacterial growth inhibition (after 4h incubation time) caused by AgNPs and CAC/AgNPs led us to the conclusion that both nanomaterials induced a bacteriostatic effect as the bacterial growth resumed after 10 h of incubation and beyond. Noteworthy, the growth inhibition was concentration dependent as the more the MIC value (2MIC and 4MIC), the higher was the inhibition as evidenced by the trend of curves presented in Figure 7 & 8. However, ciprofloxacin, which was used as positive control did not show the same trend as this compound inhibited the bacterial growth in a continuous manner, whereas the untreated control group displayed an exponential growth of bacteria from 0 to 24 h (Figures 7 and 8).

Preprints (www.preprints.org) | NOT PEER-REVIEWED | Posted: 25 October 2023 doi:10.20944/preprints202310.1616.v1

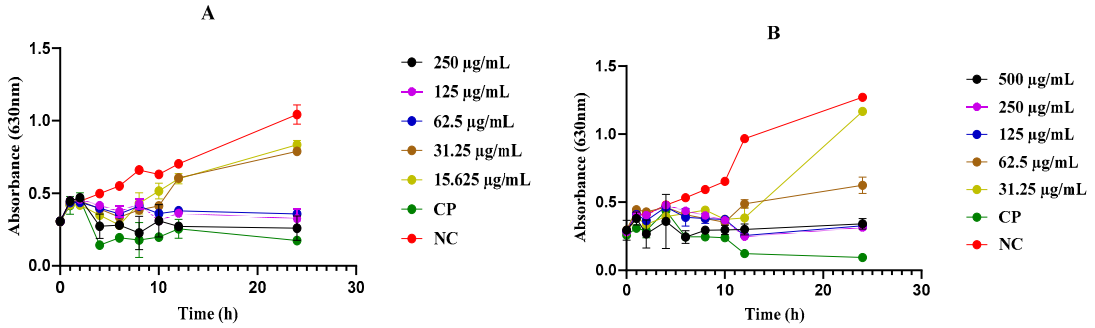

(**A**) **:** Growth curve of *E. coli;* (**B**): *S. aureus*; **CP**: Ciprofloxacin; **NC**: Negative control; Data are represented as mean ± standard deviation; Significant difference compared with negative control ($P < 0.05$, Tukey).

Figure 7. Growth inhibition kinetics of the nanoparticles (AgNPs) against bacterial strains**.**

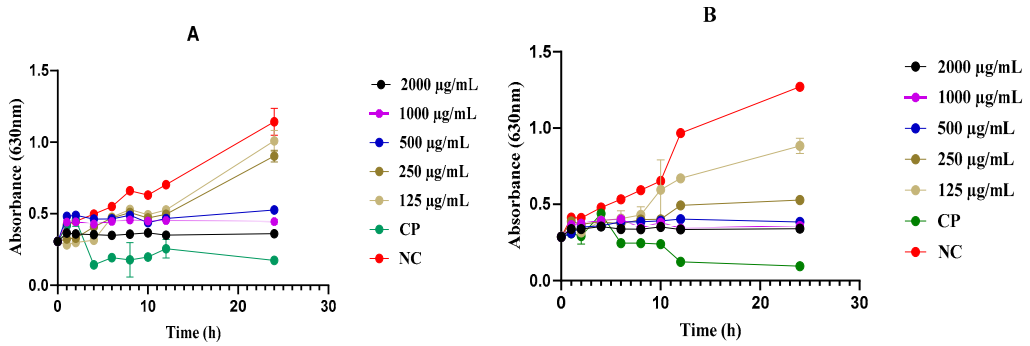

(**A**) **:** Growth curve of *E. coli*, (**B**) Growth curve of *S. aureus*, **CP**: Ciprofloxacin, **NC**: Negative Control, Data are represented as mean ± standard deviation, Significant difference compared with negative control ($P < 0.05$, Tukey).

Figure 8. Growth inhibition kinetics of the nanocomposite (CAC/AgNPs) against bacterial strains**.**

2.6. Effect of Nanomaterials on the Membrane Integrity of Escherichia coli and Staphylococcus aureus

To evaluate the effect of the as-prepared nanomaterials on the bacterial membrane integrity, cells were treated with MIC value-based concentrations (MIC/2, 2MIC and MIC) and incubated at incubation times varying from 0 to 8 h (0, 0.5, 1, 2, 4, 6 and 8 h). Next, the absorbance was measured at 260 nm (wavelength at which nucleic acid absorbs ultraviolet light) after 8 h of incubation time. Irrespective of the concentration tested, there was no significant leakage of nucleic acids following bacterial treatment with AgNPs (Figure 9 A&C) and CAC/AgNPs (Figure 9 B & D). This observation suggests that the antibacterial mechanism of action of the as-prepared nanomaterials is far from being through cell membrane disruption. However, due to their nanoscale size, nanomaterials anchor onto and easily penetrate and pass through the cell wall and interact with the cell organelles [58,59]. Once in the bacteria, the nanomaterials interacts with proteins, lipids, DNA lysosomes, ribosomes, and enzymes to inhibit the normal cell function (oxidative stress, heterogeneous alterations, enzyme inhibition, changes in gene expression, among others) [28,60,61]. Although detailed antibacterial mechanisms of nanomaterials have not been fully unveiled, other reports point out the (i) induction of oxidative stress, (ii) release of the metal and metal oxide ions, (iii) and non-oxidative mechanisms [28,62].

Preprints (www.preprints.org) | NOT PEER-REVIEWED | Posted: 25 October 2023 doi:10.20944/preprints202310.1616.v1

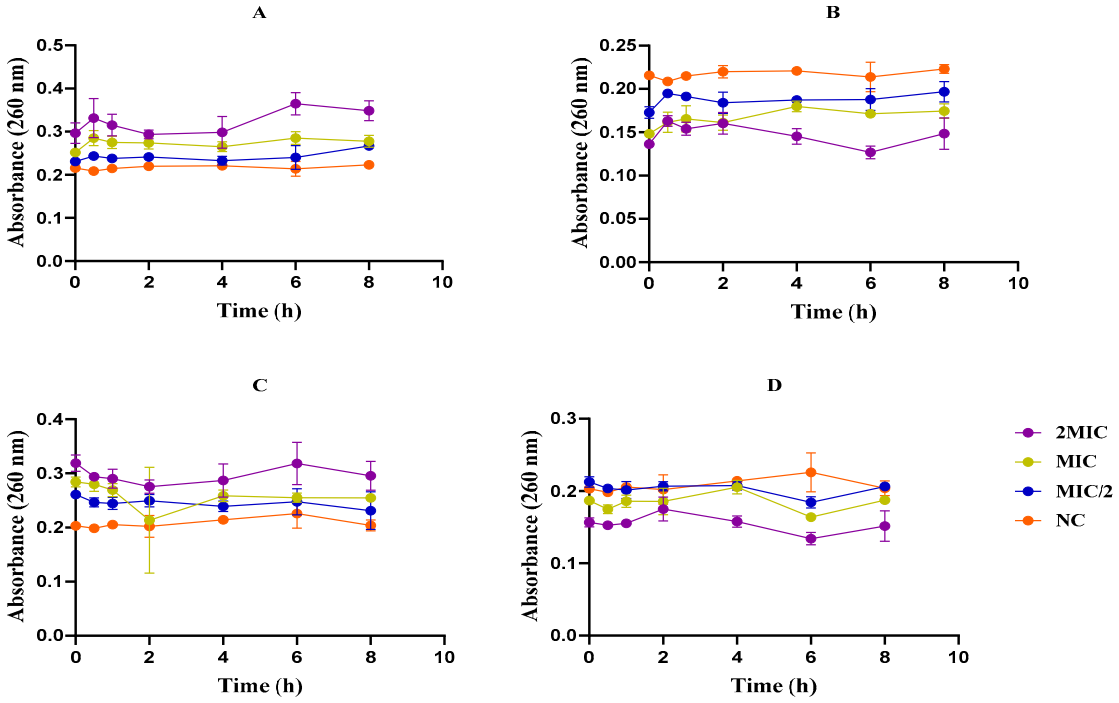

A: AgNPs on *S. aureus*, **B**: CAC/AgNPs on *S. aureus*, **C**: AgNPs on *E. coli*, **D**: CAC/AgNPs on *E. coli*, **AgNPs**: silver nanoparticles, **CAC/AgNPs**: nanocomposite, **EC**: *Escherichia coli*, **MIC**: minimum inhibitory concentration, **NC**: Negative control, **SA**: *Staphylococcus aureus*. Data are represented as mean ± standard deviation. No significant difference when compared with the negative control at $p < 0.05$.

Figure 9. Effect of nanocomposite (CAC/AgNPs) and nanoparticles (AgNPs) on nucleic acid release in bacteria.

2.7. Catalase Inhibition Assay of the Nanomaterials

To evaluate the activity of catalase in *E. coli* and *S. aureus*, cells were treated with AgNPs and CAC/AgNPs along with hydrogen peroxide and PBS (phosphate buffer saline) for 30 min [63]. After reading the optical densities of the supernatant (obtained via centrifugation of the incubated preparation), the percentage of remaining H_2O_2 was calculated. In *E. coli*, the percentages of H_2O_2 remaining in the bacterial cultures after treatment varied from 2.45 to 6.02%, whereas in *S. aureus*, these values ranged from 17.26 to 24.20% (Figure 10). Notably, the activity of the nanocomposites on catalase produced by both bacteria was superior as compared to that of the nanoparticles. Widely distributed in aerobic and some anaerobic bacteria, catalase is an enzyme that is crucial in bacterial defense against oxidative stress [64,65]. Thus, it is not unreasonable to speculate that the as-prepared nanomaterials might have exerted antibacterial action by inhibiting the activity of catalase in *E. coli* and *S. aureus*.

Preprints (www.preprints.org) | NOT PEER-REVIEWED | Posted: 25 October 2023 doi:10.20944/preprints202310.1616.v1

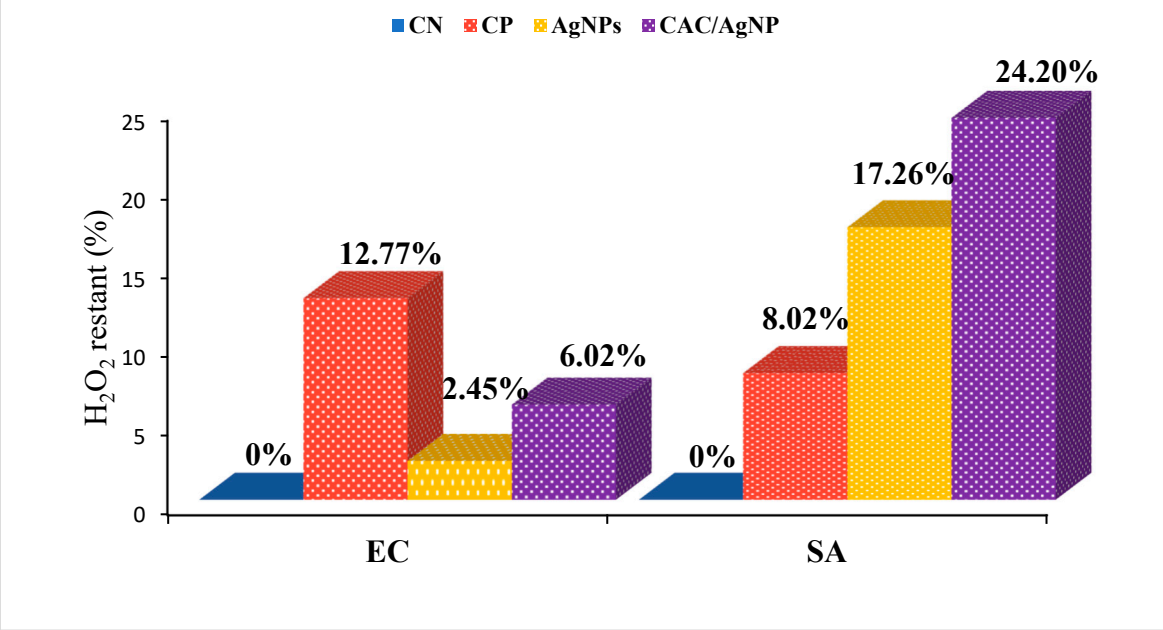

AgNP: Nanoparticles, **CAC/AgNP:** nanocomposite, **CP:** Ciprofloxacin, **EC:** *Escherichia coli*, **CN :** Negative Control, **SA:** *Staphylococcus aureus*. Data are represented as mean ± standard deviation.

Figure 10. Effect of silver nanoparticles and nanocomposite on the catalase activity in *Escherichia coli* and *Staphylococcus aureus*.

3. Material and Methods

3.1. Plant Collection and Identification

The plant material consisted of bark from the trunk of *Croton macrostachyus* that was collected at Baneghang (West Region, Cameroon) in March 2021. The identity of the plant was confirmed by Mr Nana Victor (Botanist) at the National Herbarium of Cameroon (Yaounde, Cameroon), where a voucher specimen was deposited under number 32264HNC.

3.2. Plant Extraction

The collected plant material was shade dried, then ground to fine powder using a grinder. Next, 10 g of bark powder was added to 500 mL of distilled water in an Erlenmeyer flask and boiled on a hot plate for 10 min. The resulting solution was allowed to cool to room temperature, then filtered through Wattman paper N°1 and the filtrate was dried under ventilation for 4 days and the extract was collected and kept at 4°C for future use.

3.3. Preparation of Activated Carbon from Croton Macrostachyus

The stem bark of *Croton macrostachyus* was washed with distilled water, cut into small pieces and dried at room temperature (25°C) in the dark. Next, the dried samples were ground and sieve to obtain finer particles. Ten grams (10 g) of the fine powder (CMP) was impregnated with H_3PO_4 solution (1:1). The reaction mixture was left at room temperature for 1 h to allow for a complete absorption into the *C. macrostachyus* stem bark. Afterward, the impregnated *C. macrostachyus* stem bark was dried at 110°C for 24 h in an oven. The dried samples were kept temporarily in the desiccator, then carbonized at 432°C for 40 min using a Carbolite Furnace to obtain the activated carbon (CAC).

 doi:10.20944/preprints202310.1616.v1

3.4. Biological Synthesis and Characterization of Silver Nanoparticles Using Croton Macrostachyus

3.4.1. Preparation of Silver Nanoparticles

For the synthesis of nanoparticles (AgNPs), 10 g of fine bark powder was added to 500 mL of distilled water in an Erlenmeyer flask and boiled on a hot plate for 10 min. The resulting solution was allowed to cool to room temperature, and then filtered using Wattman paper number 1. One hundred milliliters (100 mL) of the obtained aqueous extract was added to 100 mL of 5 mM aqueous silver nitrate ($AgNO_3$) solution. Next, the mixture was stirred for 1 min using a magnetic stirrer (Horse shoe IKA magnetic agitator) in the absence of light to avoid any photochemical reactions of silver nitrate and stored in a dark chamber for 24 h. The generation of the nanoparticles was evidenced by the color change from pale yellow to dark brown. The absorbance of the resulting solution was read using a visible ultraviolet spectrophotometer.

3.4.2. Characterization of AgNPs

The as-prepared silver nanoparticles were characterized using analytical techniques, such as UV-visible (UV–Vis) spectrophotometry and Fourier transform infrared (FTIR).

3.4.2.1. UV-Vis Spectrophotometry Analysis

The UV-visible analysis of the extracts, and prepared nanoparticles (AgNPs) was carried out using shimadzu UV-visible spectrophotometer (UV-1800, Japan) in the wavelength range of 350–900 nm to obtain the UV-visible spectra of the sample.

3.4.2.2. Fourier Transform Infrared Spectroscopy Analysis of AgNPs

FTIR analysis of the aqueous extract and AgNPs was performed in the absorbance range of 400 to 4000 cm-1 using a Universal ATR, Crystal: Platinum, Diamond, Bounces: 1, Solvent: ethanol. In brief, the prepared extract or nanoparticles (AgNPs) were mixed with potassium bromide (KBr) and subsequently pressed into pellets. The pellets thus formed by compression were placed in the sample holder of the apparatus for analysis. The results of the transmittance as a function of the wavelengths were given by the screen. Afterwards, the obtained spectrograms were analyzed to identify the functional groups located on the surface of extracts and nanoparticles.

3.5. Preparation and Characterization of Nanocomposite from Croton Macrostachyus

3.5.1. Preparation of the Nanocomposite

To obtain the nanocomposites (CAC/AgNPs), the silver nanoparticles (AgNPs) were loaded on the activated carbon (CAC) by means of simple agitation. Briefly, 5.0 g of CAC was added to AgNPs solution, then the resulting solution was vigorously mixed by continuous stirring for 1 h at 150 rpm using a Horse shoe IKA agitator. The nanocomposite was obtained by drying the AgNPs-loaded activated carbon powder at 110°C in an oven (Bluepard Instruments Co. Ltd, Shangai).

3.5.2. Characterization of the Adsorbents Activated Carbon and Nanocomposite

The as-prepared activated carbon (CAC) and nanocomposite (CAC/AgNP) were characterized by determination of methylene blue and iodine numbers. FTIR measurements were carried out to detect changes in the composition of biomolecules and their functional groups. FTIR analysis was performed in the absorbance range of 400 to 4000 cm-1 using Universal ATR, Crystal: Platinum, Diamond, Bounces:1, Solvent: ethanol.

3.5.3. Determination of the Methylene Blue Index and Iodine Number

Defined as the number of milligrams of iodine or methylene blue adsorbed by 1 g of activated carbon, iodine number and methylene blue index, respectively provide information on the

Preprints (www.preprints.org) | NOT PEER-REVIEWED | Posted: 25 October 2023 doi:10.20944/preprints202310.1616.v1

microporosity (up to 2 nm) and mesoporosity of the activated carbon. The porosity of the activated carbon is critical to conclude about the degree of adsorption of metal loaded-activated carbon of molecular size.

3.5.3.1. Determination of the Iodine Number Using Batch Mode Adsorption

To determine the iodine number, 100 mg of CAC and CAC/AgNPs were separately introduced into 30 mL of iodine solution in 100 mL Erlenmeyer flasks. Then, the mixtures were sealed and stirred for 3 h at room temperature. After stirring, each mixture was filtered through a Wattman filter paper and the filtrate obtained was collected in a dry flask.

Next, 10 mL of each solution was titrated with sodium thiosulfate using starch as an indicator until the solution became transparent. The equation for of this the reaction is as follows:

The amount of iodine adsorbed is given by the reaction following formula (Nasehir et al., 2010) [66]:

$$Q=\frac{(Co-Ce)\times V}{m_{CAP}}$$

Where Co is the initial concentration of methylene blue ; Ce is the equilibrium concentration of the methylene blue ; m represents the mass (g) of sample (CAC or CAC/AgNPs) ; and V is the volume of methylene blue solution.

3.5.3.2. Determination of the Methylene Blue Index Using Batch Mode Adsorption

To determine the methylene blue index, 100 mg of CAC and CAC/AgNPs were separately introduced into 30 mL of methylene blue solution in 100 mL Erlenmeyer flasks. Then, the mixtures were sealed and stirred for 3 h at room temperature. After stirring, each mixture was filtered using a Wattman filter paper number 1 and the filtrate obtained was collected in a dry flask. Next, the absorbance was read at 660 nm against the blank using a spectrophotometer (Spectrumlab S23A). The amount of methylene blue adsorbed was calculated using the following formula [66]:

$$Q=\frac{(Co-Ce)\times V}{m_{CAP}}$$

Where Co is the initial concentration of methylene blue ; Ce is the equilibrium concentration of the methylene blue ; m represents the mass (g) of sample (CAC or CAC/AgNPs) ; and V is the volume of methylene blue solution.

3.6. Antibacterial Activity

The antibacterial activity of the *C. macrostachyus* extract and synthesized nanomaterials was assessed on five bacterial strains according to the guidelines set by the Clinical Laboratory Standards Institute [67] using 96-well microtitre plates. The bacterial strains used in this study are summarized in Table 2. *Shigella flexneri* and *Shigella sonnei* were generously obtained from the Biodefense and Emerging Infections Research Resources Repository (BEI Resources, Rockville, MD 20,852), whereas *Escherichia coli* and *Staphylococcus aureus* was obtained commercially from the American Type Culture Collection (ATCC, Manassas, VA, USA). *Salmonella enteridis* was generously obtained from the Centre Pasteur of Cameroon (CPC).

Table 2. List of bacterial strains used for anti-bacterial activity.

Bacterial strains	Acronym	Reference number	Supplier
Escherichia coli	*E. coli*	ATCC 25922	ATCC
Salmonella enteridis	*S. enteridis*	Isolat	CPC

 doi:10.20944/preprints202310.1616.v1

Shigella flexneri	*S. flexneri*	NR 518	BEI resources
Shigella sonnei	*S. sonnei*	NR 519	BEI resources
Staphylococcus aureus	*S. aureus*	ATCC 43300	ATCC

ATCC, American Type Culture Collection; **BEI Resources**, Biodefense and Emerging Infections Research Resources Repository, **CPC,** Centre Pasteur of Cameroon.

Briefly, 96 µL of Mueller Hinton Broth (MHB) culture medium was introduced into each well of a 96 well plate followed by a subsequent addition of 4 µL of stock solution of each prepared sample (extract of AgNPs) at 100 mg/mL. Next, 100 µL of 1 x 10^6 mL of inoculum was added to each well except those for the sterility control. The positive control consisted of the inoculum and ciprofloxacin (10 µg/mL). The negative control comprised culture medium and inoculum, whereas the sterility control consisted of culture medium only. The plates were covered and incubated at 37°C for 24 h. At the end of the incubation period, 20 µL of freshly prepared resazurin solution (0.15 mg/mL) was added to each well and the plates were once again incubated under the same conditions for 30 min. The wells in which there was no visible bacterial growth corresponded to those containing active substances. Extracts and nanoparticles that inhibited the growth of bacteria at 1000 µg/mL concentration were selected for the determination of the minimum inhibitory concentrations (MICs).

3.7. Determination of the Minimum Inhibitory Concentrations

The minimum inhibitory concentrations (MICs) of the doped activated carbons and nanoparticles from *C. macrostachyus* were determined by the broth microdilution method, using the microdilution assay as described above. The assays were performed in duplicate in sterile 96-well microplates. In brief, 196 µL of MHB culture medium was introduced into the wells of column A, while 100 µL were added into the remaining wells of the microplate. Subsequently, 4 µL of a sterile solution of extract or nanoparticle (AgNPs), or nanocomposite (CAC/AgNPs) (100 mg/mL) was added into the wells of column A. This addition was followed by a series of 8 dilutions in geometric reasoning of order 2 and from column A to H. Next, 100 µL of bacterial load *viz*. 1x10^6 UFC/mL was distributed to the remaining wells, including negative control wells. The concentrations of extract or nanoparticles, and ciprofloxacin in the wells of a row ranged from 1000 µg/mL to 7.8125 µg/mL, and from 5 µg/mL to 0.15625 µg/mL, respectively. The sterility control contained the culture medium only, whilst the positive group was made up of culture medium, inoculum and ciprofloxacin (stock solution at 1 mg/ml). The microplates were coated and then incubated at 37°C for 24 h. Next, 20 µL of freshly prepared resazurin solution (0.15 mg/mL) was added to all wells and the plates were incubated again at 37°C for 30 min. The lowest concentrations at which no color change (from blue to pink) were observed corresponded to absence of bacterial growth and were considered as MIC values.

3.8. Cytotoxicity Assays

The cytotoxicity of the most active nanomaterials was assessed on human mammalian cells (Vero cell line ATCC CRL 1586) using the resazurin colorimetric method as described by Bowling et al. [68]. The Vero cell line (ATCC CRL 1586) were cultured in complete medium containing 13.5 g/L DMEM (Gibco, Waltham, MA USA), 0.5% MEM (Gibco, Waltham, MA USA), 10% fetal bovine serum (Gibco, Waltham, MA USA), 0.21% bicarbonate (Sigma-Aldrich, New Delhi, India), and 10 mL (1%) of penicillin/streptomycin antibiotics. Briefly, 100 µL of cell suspension was introduced into 96-well (Costar, USA) microplates (10^4 cells per well) and incubated overnight (18 h) to allow cell adhesion. Subsequently, the culture medium was replenished with 90 µL of new fresh complete culture medium, and then 10 µL of serially diluted extract or nanoparticles were added in triplicate to the corresponding wells. Podophyllotoxin at 50 µM was used as a positive control, and wells involving untreated cells were included as a 100% growth control. Next, the plates were incubated in a humidified atmosphere with 5 % CO_2 at 37°C for 48 h. Afterwards, 10 µL of resazurin stock solution

Preprints (www.preprints.org) | NOT PEER-REVIEWED | Posted: 25 October 2023 doi:10.20944/preprints202310.1616.v1

(0.15 mg/mL in phosphate buffer saline, PBS) was added to each well and incubated for an additional 4 h. Fluorescence was then read using a multi-well plate reader (TECAN-Infinite M200) at excitation and emission wavelengths of 530 et 590 nm, respectively. From the optical densities (OD) obtained, the percentages of cell viability were calculated according to the following formula :

$$\textbf{Percentages of cell viability } (\%) = \frac{\textbf{OD test}}{\textbf{OD negative control}} \times \textbf{100}$$

Percentages of cell viability were used to determine the median cytotoxic concentrations (CC_{50}) using nonlinear regression curves using GraphPad Prism 5.0 (San Diego, Californie) software. ‘

3.9. Potential Mechanistic Studies of the Most Potent Nanomaterials

To understand the mechanism of antibacterial action, the growth kinetics, release of nucleic acids by bacteria and inhibition of catalase upon treatment with the most promising nanoparticules (AgNPs) and nanocomposite (CAC/AgNPs) were investigated.

3.9.1. Bacterial Growth Kinetics on Various Concentrations of the Nanomaterials

To study the bacterial growth curve, cultures containing *E. coli* and *S. aureus* strains were incubated with the most active antibacterial nanoparticles (AgNPs) and nanocomposites (CAC/AgNPs) as per the protocol reported by Nguimatsia et al. [69] with minor modifications. In short, 20 µL of AgNPs and 8 µL of CAC/AgNPs were added respectively in 180 µL and 192 µL of Mueller Hinton Broth in the first twelve wells of column A (A). In the remaining wells of the microplate, 100 µL of Mueller Hinton Broth was introduced. Next, a series of geometric dilutions of order 2 was operated from column A to H to achieve concentrations ranging from 250 to 15.625 µg/mL and from 2000 to 125 µg/mL for AgNPs and CAC/AgNPs, respectively. Afterwards, 100 µL of $1x10^6$ UFC/mL inoculum was introduced into each well except for control groups (sterility, AgNPs and CAC/AgNPs). Ciprofloxacin was used as a positive control. The microplate was coated and incubated at 37°C at diverse incubation time periods (0, 1, 2, 4, 6, 8, 10, 12 and 24 h) and the optical densities were read at 630 nm using a microplate reader (Infinite M200 microplate reader TECAN, Männedorf, Switzerland) after each incubation time was elapsed. The values obtained were used to plot OD = f(t) graphs.

3.9.2. Nucleic Acid Leakage Assays

This test was performed according to the protocol described by Carson et al. [70]. The assays were performed in triplicate in 2 mL eppendorf tubes. Colonies obtained from 24 h cultures were washed twice with NaCl solution (0.9%), then resuspended in sterile peptone water (0.1%) and calibrated to 0.5 MacFarland standard. Subsequently, 250 µL of inoculum (1.5×10^8 UFC/mL) was introduced into 250 µL of peptone water containing the prepared extract at different concentrations including 2CMI, CMI et CMI/2, and the the tubes were incubated at 37°C at different times (0, 0.5, 1, 2, 4, 6 and 8 h). After each incubation period, the solution was centrifuged at 5000 rpm for 20 min. The supernatant was collected and transferred into wells of a microplate and the absorbance was measured at 260 nm using a TECAN infinite M200 plate reader. The obtained optical densities (OD) were plotted versus time using Excel software.

3.9.3. Catalase Inhibition Assay

The catalase inhibition assay of the most active nanoparticles (AgNPs) or nanocomposites (CAC/AgNPs) was determined on *E. coli* ATCC 25922 and *S. aureus* ATCC 43300, according to a previously described protocol [63]. The assays were performed in triplicate in 2 mL eppendorf tubes. Various concentrations of samples (AgNPs and CAC/AgNPs) were introduced in test tubes containing 200 µL of hydrogen peroxide (40 mM) and 200 µL of phosphate buffer saline (PBS 10X; pH= 7.3 – 7.7) (Sigma-Aldrich, Germany). Next, In the mixture, 100 µL of bacterial suspension at 1.5×10^8 CFU/mL were added and the samples were incubated at 37°C for 30 min. Then, the test tubes were centrifuged at 1200 rpm for 10 min and the supernatants were further collected and transferred

Preprints (www.preprints.org) | NOT PEER-REVIEWED | Posted: 25 October 2023 doi:10.20944/preprints202310.1616.v1

into wells of a microplate. At last, the optical density of the microplate was read against the blank (phosphate buffer saline, PBS 10X, pH : 7.3-7.7) and the negative control (bacteria in PBS without inhibitor) at 232 nm using an Infinite M200 microplate reader (TECAN, Männedorf, Switzerland). Ciprofloxacin (at 0.078 and 0.039 µg/mL for *E. coli* ATCC 25922 and *S. aureus* ATCC 43300, respectively) was used as a positive control. The percentage of remaining hydrogen peroxide was determined according to the following formula :

$$\% \text{ de } H_2O_2 \text{ restant} = \frac{(Ae - Ac)}{Ac} \times 100$$

Ac is the negative control, whereas Ae is the absorbance of H_2O_2 in the presence of the sample.

3.9.4. Statistical Analysis

Results were expressed as mean ± standard deviation. The statistical analysis and plots were performed using Graphpad Prism 8 and Excel software. The means were analyse using one-way ANOVA (Analysis of variance) test, followed by a post hoc multiple comparison (Tukey test) and were considered significant for *P < 0.05, **P < 0.01, ***P < 0.001 and ****P < 0.0001.

4. Conclusion

To sum up, an eco-friendly method was developed to synthesize silver nanocomposite from the corresponding nanoparticle and *C. macrostachyus*-based activated carbon. The nanomaterials were further characterized using UV-visible spectroscopy, and FTIR analyses. The nanomaterials exhibited antibacterial activity against an array of bacterial strains, the most susceptible being *Escherichia coli* and *Staphylococcus aureus*. Although the activated carbon did not exhibit antibacterial action, their role in minimizing the cytotoxicity of the nanocomposite was paramount. Antibacterial mechanistic studies revealed that the as-prepared nanomaterials induced (i) bacteriostatic activity vis-à-vis *E. coli* and *S. aureus* and (ii) inhibition of catalase in these bacteria. This novel contribution on the antibacterial mechanisms of action of silver nanocomposite from *C. macrostachyus*-based activated carbon might help in better understanding the bacterial inhibition by this biomaterial. The results suggest that the prepared nanocomposite could be a promising antibacterial potential candidate with low toxicity to Vero cells.

Author Contributions: "Conceptualization, P.K.L., J.N.N. and F.F.B; methodology, P.K.L., J.N.N., F.L.T.T., BPK, VLY, and ZYT; software, F.L.T.T.; validation, P.K.L., J.N.N., and F.F.B.; formal analysis, F.L.T.T., ZYT, VLY, B.P.K. and N.V.; investigation, F.L.T.T., B.P.K and NV; resources, P.K.L., J.N.N. and F.F.B; data curation, F.L.T.T., B.P.K, and N.V.; writing—original draft preparation, F.L.T.T., B.P.K. and N.V.; writing—review and editing, F.L.T.T., B.P.K. and V.N.; visualization, P.K.L.; supervision, P.K.L., J.N.N. and F.F.B; project administration, P.K.L., J.N.N., B.P.K. and F.F.B; funding acquisition, P.K.L., J.N.N. and F.F.B. All authors have read and agreed to the published version of the manuscript."

Funding: "This research received external funding from the Yaounde-Bielefeld Bilateral Graduate School for Natural Products with Anti-parasite and Antibacterial Activity (YaBiNaPA) (grant number 57316173) and the Seeding Labs' Instrumental Access".

Institutional Review Board Statement: Not applicable.

Informed Consent Statement: Not applicable.

Data Availability Statement: Data is available from the corresponding author upon reasonable request.

Acknowledgments: Authors are thankful to the Cameroon National Herbarium (Yaounde, Cameroon) for the plant's identification. The authors also acknowledge the ''Centre Hospitalier Universitaire'' of Yaounde-Cameroon and ''Centre Pasteur'' of Cameroon for providing the bacterial strains species. This work was supported by also received materials and equipment support from the Yaoundé-Bielefeld Bilateral Graduate School for Natural Products with Anti-parasite and Antibacterial Activity (YaBiNaPA) and the Seeding Labs' Instrumental Access.

Conflicts of Interest: The authors declare no conflict of interest.

References

1. The World Health Organization (WHO), 2023a. Shigella. The Fact Sheets. https://www.who.int/teams/immunization-vaccines-and-biologicals/diseases/shigella, Accessed on 05th October 2023.
2. Cleveland Clinic (CC), 2023. Infectious diseases. *https://my.clevelandclinic.org/health/diseases/17724-infectious-diseases,* Accessed on 07th October 2023.
3. The World Health Organization (WHO), 2023b. The Key Facts. Antibiotic resistance. https://www.who.int/news-room/fact-sheets/detail/antibiotic-resistance, Accessed on 06th October 2023.
4. Reygaert, W.C. An overview of the antimicrobial resistance mechanisms of bacteria. AIMS Microbiol. **2018**, 4 (3) 482-501.
5. Neu, H.C.; Gootz, T.D. Basis of Antimicrobial Action; General Concepts; Medical Microbiology. Chapter 11: Antimicrobial Chemotherapy. Baron S, editor. Medical Microbiology. 4th edition. Galveston (TX): University of Texas Medical Branch at Galveston; **1996**, 1-17.
6. Jeśman, C.; Młudzik, A.; Cybulska, M. Historia odkrycia antybiotyków i sulfonamidów [History of antibiotics and sulphonamides discoveries]. *Pol. Merkur. Lekarski*. **2011**, *30 (179)* 320-322.
7. Bhattacharjee, M.K. Antimetabolites : Antibiotics that inhibit nucleotide synthesis. Book Chapter. Chemistry of Antbiotics and Related Drugs. **2016**, pp 109–123.
8. Estrada, A.; Wright, D.L.; Anderson, A.C. Antibacterial antifolates: From development through resistance to the next generation. *Cold Spring Harb Perspect Med.* **2016**, *6(8)* a028324.
9. Fisher, J.F.; Mobashery, S. β-Lactams from the Ocean. *Mar Drugs* **2023**, *21* (2) 1-15.
10. Smith, P.W.; Zuccotto, F.; Bates, R.H.; Martinez-Martinez, M.S.; Read, K.D.; Peet, C.; Epemolu, O. Pharmacokinetics of β-lactam antibiotics: Clues from the past to help discover long-acting oral drugs in the future. *ACS Infect. Dis.* **2018**, *4(10)* 1439-1447.
11. Cambau, E.; Guillard, T. Antimicrobials that affect the synthesis and conformation of nucleic acids. *Rev. Sci. Tech.* **2012**, *31(1)* 77-87, 65-76.
12. Fernández-Villa, D.; Aguilar, M.R.; Rojo, L. Folic acid antagonists: Antimicrobial and immunomodulating mechanisms and applications. *Int. J. Mol. Sci.* **2019**, *20(20)* 4996.
13. Kannan, K.; Mankin, A.S. Macrolide antibiotics in the ribosome exit tunnel: species-specific binding and action. *Ann. N. Y. Acad. Sci.* **2011**, *1241*, 33-47.
14. Aslam, B.; Wang, W.; Arshad, M.I.; Khurshid, M.; Muzammil, S.; Rasool, M.H.; Nisar, M.A.; Alvi, R.F.; Aslam, M.A.; Qamar, M.U.; Salamat, K.F.; Baloch Z. Antibiotic resistance: a rundown of a global crisis. *Infect. Drug Resist.* **2018**, *11*, 1645-1658.
15. Ghosh, A.; Jayaraman, N.; Chatterji, D. Small-molecule inhibition of bacterial biofilm. *ACS Omega* **2020**, *5(7),* 3108-3115.
16. World Health Organisation (WHO). WHO methods and data sources for global burden of disease estimates 2000-2011. *Geneva: Department of Health Statistics and Information Systems*, **2013**.
17. Tang, S.; Zheng, J. Antibacterial activity of silver nanoparticles: Structural effects. *Adv. Healthc. Mater.* **2018**, *1701503*, 1-10.
18. Ugboko, H.U. ; Nwinyi, O.C. ; Oranusi, S.U. ; Fatoki, T.H. ; Omonhinmin, C.A. 2020. Antimicrobial importance of medicinal plants in Nigeria. *Sci. World J.* **2020**, 1-10.
19. Abdallah, E.M.; Alhatlani, B.Y.; Menezes, R. de P.; Martins, C.H.G. Back to nature: Medicinal plants as promising sources for antibacterial drugs in the post-antibiotic era. *Plants* **2023**, *12(17),* 3077.
20. Mody V.V.; Siwale, R.; Singh, A.; Mody, H.R. Introduction to metallic nanoparticles. *J. Pharm. Bioallied Sci.* **2010**, 2, 282-289.
21. Zomuansangi, R.; Singh, B.P.; Singh, G.; Puia, Z.; Singh, P.K.; Song, J.J.; Kharat, A.S.; Deka, P.; Yadav, M.K. Chapter 14 - Role of nanoparticles in the treatment of human disease: a comprehensive review. Nanotechnology and Human Health. Current Research and Future Trends. Nanotechnology in Biomedicine. **2023**, Pages 381-404.
22. Makvandi, P.; Wang, C.y.; Zare, E.N.; Borzacchiello, A.; Niu, L.n.; Tay, F.R. Metal-based nanomaterials in biomedical applications: Antimicrobial activity and cytotoxicity aspects. *Adv. Funct. Mat.* **2020**, *30*, 1910021.
23. Susanti, D.; Haris, M.S.; Taher, M.; Khotib, J. Natural products-based metallic nanoparticles as antimicrobial agents. *Front. Pharmacol.* **2022**, *13*, 1-14.
24. Dolai, J.; Mandal, K.; Jana, N.R. Nanoparticle size effects in biomedical applications. *ACS Appl. Nano. Mater.* **2021**, *4 (7),* 6471–6496.

25. Chandraker, S.K.; Kumar, R. Biogenic biocompatible silver nanoparticles: a promising antibacterial agent. *Biotechnol. Genet. Eng. Rev.* **2022**, *2*, 1-35.
26. Dakal, T.C.; Kumar, A.; Majumdar, R.S.; Yadav, V. Mechanistic basis of antimicrobial actions of silver nanoparticles. *Front. Microbiol.* **2016**, *7*, 1-17.
27. Franci, G.; Falanga, A.; Galdiero, S.; Palomba, L.; Rai, L.; Morelli, G., Galdiero, M. Silver nanoparticles as potential antibacterial agents. *Molecules*, **2015**, *20* (*5*), 8856-8874.
28. Wang, L.; Hu, C.; Shao, L. The antimicrobial activity of nanoparticles: present situation and prospects for the future. *Int. J. Nanomed.* **2017**, *12*, 1227-1249.
29. Yu, L.; Tatsumi, D.; Kondo, T. Preparation of carbon nanoparticles from activated carbon by aqueous counter collision. *J. Wood Sci.* **2022**, *68*, 1-8.
30. Pongener, C.; Kibami, D.; Rao, K.S.; Goswamee, R.L.; Sinha, D. Adsorption studies of fluoride by activated carbon prepared from *Mucuna prurines* plant. *J. Water Chem. Technol.* **2017**, *39*, 108-115.
31. Burchacka, E.; Pstrowska, K.; Bryk, M.; Maciejowski, F.; Kułażyński, M.; Chojnacka, K. The properties of activated carbons functionalized with an antibacterial agent and a new SufA protease inhibitor. *Materials (Basel)* **2023**, *16*(*3*), 1-18.
32. Rivera-Utrilla, J.; Bautista-Toledo, I.; Ferro-Garca, M.A.; Moreno-Castilla, C. 2001. Activated carbon surface modifications by adsorption of bacteria and their effect on aqueous lead adsorption. *J. Chem. Technol. Biotechnol.* **2001**, 76, 1209-1215.
33. Balashanmugam, P.; Kalaichelvan, P.T. Biosynthesis characterization of silver nanoparticles using *Cassia roxburghii* DC. aqueous extract, and coated on cotton cloth for effective antibacterial activity. *Int. J. Nanomed.* **2015**,*10 Suppl 1*(*Suppl 1*) 87-97.
34. Wibawa, P.J.; Nur, M.; Asy'ari, M.; Wijanarka, W.; Susanto, H.; Sutanto, H.; Nur, H. Green synthesized silver nanoparticles immobilized on activated carbon nanoparticles: Antibacterial activity enhancement study and its application on textiles fabrics. *Molecules* **2021**, *26*(*13*), 3790.
35. Ameen, F.; Karimi-Maleh, H.; Darabi, R.; Akin, M.; Ayati, A.; Ayyildiz, S.; Bekmezci, M.; Bayat, R.; Fatih, S. Synthesis and characterization of activated carbon supported bimetallic Pd based nanoparticles and their sensor and antibacterial investigation. *Environ. Res.* **2023**, 221, 115287.
36. Sastry, M.; Mayya, K.S.; Bandyopadhyay, K. pH Dependent changes in the optical properties of carboxylic acid derivatized silver colloidal particles. *Colloids Surf. A: Physicochem. And Engi. Aspect* **1997**, 127, 221-228.
37. Kathiravan, V.; Ravi, S.; Ashokkumar, S.; Velmurugan, S.; Elumalai, K.; Khatiwada, C.P. Green synthesis of silver nanoparticles using *Croton sparsiflorus* morong leaf extract and their antibacterial and antifungal activities. *Spectrochim. Acta Part A Mol. Biomol. Spectrosc.* **2015**, *139*, 200-205.
38. Kapoor, R.T. Biosynthesis and characterization of silver nanoparticles from *Croton bonplandianum* Baill and its antioxidant activity. *Int. J. Pharm. Res. Allied Sci.* **2015**, *4*(*4*), 39-44.
39. Oladotun, P.B.; Anuoluwa, A.A.; Adeyemi, A.O.; Williams, A.B.; Benson, N.U. Dataset on phytochemical screening, FTIR and GC-MS characterisation of *Azadirachta indica* and *Cymbopogon citratus* as reducing and stabilising agents for nanoparticles synthesis. *Data Br.* **2018**, *20*, 917-926.
40. Shaheen,, G.; Ashfaq, A.; Khawar, A.; Jamil, Q.A.; Parveen, R.; Hadi, F.; Ghauri, O.; Shirazi, J.H.; Asif, H.M.; Shamin, T.; Sumreen, L.; Ali, T.; Akram, M.; Noor, R.; Mehmood, A.; Sajid, F. Fourier transform infrared spectrometer analysis and antimicrobial screening of ethanolic extract of *Operculina terpathum* from cholistan desert. *Pharm. Pract. (Granada)* **2022**, *20*(2), 1-6.
41. Wongsa, P.; Phatikulrungsun, P.; Prathumthong, S. FT-IR characteristics, phenolic profiles and inhibitory potential against digestive enzymes of 25 herbal infusions. *Sci. Rep.* **2022**, *12*(*1*), 1-11.
42. Ganesan, V.; Deepa, B.; Nima, P.; Astalakhmi. Bio-inspired synthesis of silver nanoparticles using leaves of *Millingtonia hortensis*. *Int. J. Adv. Biotechnol. Res.* **2014**, 5(2), 93-100, 2014.
43. Moteriya, P.; Chanda, S. Biosynthesis of silver nanoparticles formation from *Caesalpinia pulcherrima* stem metabolites and their broad spectrum biological activities. *J. Genet. Eng. Biotechnol.* **2018**, 16 (1) 105-113.
44. Rahim, K.A.; Mahmoud, S.Y.; Ali, A..; Almaary, K.S.; Mustafa, A.B.Z.M.A.; Husseiny, S.M. 2017. Extracellular biosynthesis of silver nanoparticles using *Rhizopus stolonifer*. *Saudi J. Biol. Sci.* **2017**, *24* (*1*), 208-216.
45. Odogu, A.N.; Daouda, K.; Keilah, L.P.; Tabi, G.A.; Rene, L.N.; Nsami, N.J.; Mbadcam, K.J. Effect of doping activated carbon based *Ricinodendron heudelotti* shells with AgNPs on the adsorption of indigo carmine and its antibacterial properties. *Arab. J. Chem.* **2020**, *13*(*5*) 5241-5253.

46. Radičić, R.; Maletić, D.; Blažeka, D.; Car, J.; Krstulović, N. 2022. Synthesis of silver, gold, and platinum doped zinc oxide nanoparticles by pulsed laser ablation in water. *Nanomaterials (Basel)* **2022**, *12* (*19*) 1-17.
47. Tensay, G.K.; Zenebe, T.M.; Ameha, K.; Chaithanya, K.K. Phytochemical screening and evaluation of antibacterial activities of *Croton macrostachyus* stem bark extracts. *Drug Invent. Today* 2018, *10*(*1*), 2727-2733.
48. Ali, R.; Aslam, Z.; Shawabkeh, R.A.; Asghar, A.; Hussein, I.A. BET, FTIR, and RAMAN characterizations of activated carbon from waste oil fly ash. *Turk. J. Chem.* **2020**, *44*(*2*) 279-295.
49. Jaleh, B.; Fakhri, P. Chapter 5: Infrared and Fourier transform infrared spectroscopy for nanofillers and their nanocomposites. In Spectroscopy of Polymer Nanocomposites. **2016**, 112-129.
50. Asey, M.N.; Esa, N.M.; Abdullah, C.A.C. Synthesis and characterization of magnetic nanoparticles (MNP) and MNP-chitosan composites. *Malaysian J. Sci. Tech.* **2019**, *4*, 39-44.
51. Islam, M.N.; Khatton, A.; Sarker, J.; Sikder, H.A.; Chowdhury, A.M.S. 2022. Preparation and characterization of activated carbon from Jute stick by chemical activation: Comparison of different activating agents. *Saudi J. Eng. Technol.* **2022**, 7(2), 112-117.
52. Raut, E.R.; Thakur, M.A.B.; Chaudhari, A.R. 2022. Comparative study of preparation and characterization of activated carbon obtained from sugarcane bagasse and rice husk by using H_3PO_4 and $ZnCl_2$. *Mater. Today: Proc.* **2022**, *66*, 1875-1884.
53. Altammar, K.A. A review on nanoparticles: characteristics, synthesis, applications, and challenges. *Front. Microbiol.* **2023**, *14*, 1-20.
54. Ndi, N.J.; Ketcha, M.J.; Anagho, G.S.; Ghogomu, N.J.; Belibi, E. Physical and chemical characteristics of activated carbon prepared by pyrolysis of chemically treated cola nut (*Cola acuminata*) shells wastes and its ability to adsorb organics. *Int. J. Adv.Chem.Technol.* **2014**, *2014*, 2-4.
55. Pandey, P.; Karki, B.; Lekhak, B.; Koirala, A.R.; Sharma, R.K.; Pant, H.R. Comparative antibacterial study of silver nanoparticles doped activated carbon prepared by different methods. *J. Inst. Eng.* **2018**, *15*(*1*), 187-194.
56. Abongta, M.L. Effect of carbonization and doping on the antibacterial and antioxidant potentials of *Cola acuminata* shells. *Master's Thesis*, University of Yaoundé I, **2020**.
57. Sánchez-López, E.; Gomes, D.; Esteruelas, G.; Bonilla, L.; Lopez-Machado, A.L.; Galindo, R.; Cano, A.; Espina, M.; Ettcheto, M.; Camins, A.; Silva, A.M.; Durazzo, A.; Santini, A.; Garcia, M.L.; Souto, E.B. Metal-based nanoparticles as antimicrobial agents: An overview. *Nanomaterials (Basel)* **2020**, *10*(2), 1-39.
58. Chengzhu, L.; Yuchao, L.; Sie, C.T. Bactericidal and cytotoxic properties of silver nanoparticles. *Int. J. Mol. Sci.* **2019**, *20*(2), 449.
59. Ozdal, M.; Gurkok, S. Recent advances in nanoparticles as antibacterial agent. ADMET DMPK **2022**, *10*(2) 115-129.
60. Jackson, T.; Patani, B.; Israel, M. Nanomaterials and cell interactions: A review. *J. Biomater. Nanobiotechnol.* **2017**, *8*, 220-228.
61. Abarca-Cabrera, L.; Fraga-García, P.; Berensmeier, S. Bio-nano interactions: binding proteins, polysaccharides, lipids and nucleic acids onto magnetic nanoparticles. *Biomater. Res.* **2021**, *25*(*1*) 12.
62. Basavegowda N, Baek KH, 2021. Multimetallic nanoparticles as alternative antimicrobial agents: Challenges and perspectives. Molecules. 26(4) 1-21.
63. Mbekou, I.K.; Dize, D.; Yimgang, V.L.; Djague, F.; Toghueo, R.M.K., Norbert, S.; Lenta, B.N.; Boyom F.F. Antibacterial and mode of action of extracts from endophytic fungi derived from *Terminalia mantaly*, *Terminalia catappa*, and *Cananga odorata*. *Biomed Res. Int.* **2021**, (*1-9*), 2021.
64. Whittaker, J.W. Non-heme manganese catalase–the "other" catalase. *Arch. Biochem. Biophys.* **2012**, *525*, 111–120.
65. Yuan, F.; Yin, S.; Xu, Y.; Xiang, L.; Wang, H.; Li, Z.; Fan, K.; Pan, G. The richness and diversity of catalases in bacteria. *Front. Microbiol.* **2021**, *12*, 1-11.
66. Nasehir, K.E.M.; Yahaya, M.F.; Ismail, A.; Mohd A.A. Effect of preparation conditions of activated carbon prepared from rice husk by $ZnCl_2$ activation for removal of Cu (II) from aqueous solution. *Int. J. Eng. Technol.* **2010**, *10* (*6*), 27-32.
67. Clinical Laboratory Standard Institute. Methods for Dilution Antimicrobial Susceptibility Tests for Bacteria That Grow Aerobically; Approved Standard—Ninth Edition M07 A9. *Clinical Laboratory Standard Institute*. **2012**, *29*(*2*) **2012**.

68. Bowling, T.; Mercer, L.; Don, R.; Jacobs, R.; Nare, B. (2012). Drugs and drug resistance application of a resazurin-based high-throughput screening assay for the identification and progression of new treatments for human African trypanosomaisis. *Int. J. Parasitol. Drugs Drug. Resist.* **2012**, *2*, 262-270.
69. Nguimatsia, F.; Kenmogne, S.B.; Ngo-Mback, M.N.; Kouamouo, J.; Tchuitio, N.L.; Melogmo, D.Y.; Dongmo, J.P.M. Antibacterial activities of the essential oil and hydroethanolic extract from *Aeollanthus heliotropioides* Oliv. *Mediterr. J. Chem.* **2021**, *97*, 2021.
70. Carson, C.F.; Mee, B.J.; Riley, T.V. Mechanism of action of *Melaleuca alternifolia* (tea tree) oil on *Staphylococcus aureus* determined by time-kill, lysis, leakage, and salt tolerance assays and electron microscopy *Antimicrob. Agents Chemother.* **2002**, *46*, 1914–1920.